



Article

Parametric Modeling of Mass and Volume Effects for Battery Electric Vehicles, with Focus on the Wheel Components

Lorenzo Nicoletti ^{*} , Andrea Romano , Adrian König , Ferdinand Schockenhoff and Markus Lienkamp

Institute for Automotive Technology, Technical University of Munich, Boltzmannstr. 15, 85748 Garching, Germany; ge73fir@mytum.de (A.R.); adrian.koenig@ftm.mw.tum.de (A.K.); schockenhoff@ftm.mw.tum.de (F.S.); lienkamp@ftm.mw.tum.de (M.L.)

* Correspondence: nicoletti@ftm.mw.tum.de; Tel.: +49-89-289-10495

Received: 13 August 2020; Accepted: 1 October 2020; Published: 2 October 2020



Abstract: Defining a vehicle concept during the early development phase is a challenging task, since only a limited number of design parameters are known. For battery electric vehicles (BEVs), vehicle weight is a design parameter, which needs to be estimated by using an iterative approach, thus causing weight fluctuations during the early development phase. These weight fluctuations, in turn, require other vehicle components to be redesigned and can lead to a change in their size (secondary volume change) and weight (secondary weight change). Furthermore, a change in component size can impact the available installation space and can lead to collision between components. In this paper, we focus on a component that has a high influence on the available installation space: the wheels. We model the essential components of the wheels and further quantify their secondary volume and weight changes caused by a vehicle weight fluctuation. Subsequently, we model the influence of the secondary volume changes on the available installation space at the front axle. The hereby presented approach enables an estimation of the impact of weight fluctuations on the wheels and on the available installation space, which enables a reduction in time-consuming iterations during the development process.

Keywords: battery electric vehicles; secondary volume changes; secondary weight changes

1. Introduction

The CO₂ emission limits for manufacturer fleets set by the European Union (EU) have become increasingly restrictive in recent years: In 2021, the tank-to-wheel limit will be lowered to 95 g CO₂/km [1]. BEVs represent an efficient way to reduce the average fleet consumption since they do not cause any local CO₂ emissions and are accounted as 0 g CO₂/km [2].

However, for BEVs, there are currently neither established platforms nor predecessor vehicles on which the development can be based. Therefore, during the developing process of BEVs, many design parameters have to be estimated [3]. The parameter *weight* plays a key role because of the low energy density of lithium-ion-batteries compared to diesel or gasoline fuels. This can be shown by comparing an internal combustion engine vehicle (ICEV) and a BEV of the same model series (Table 1). To increase the range by 100 km, the Golf TSI (Table 1) would need an extra 4.1 L tank capacity, which results in approximately 3 kg additional weight. For the same range increase, the e-Golf would have to store 12.7 kWh more energy in the traction battery, which would result in a weight increase of approximately 127 kg, considering its actual energy density for the battery pack [4]. Correspondingly, the required battery volume increase is approximately 78 L.

Table 1. Comparison between the internal combustion engine vehicle (ICEV) [5] and the battery electric vehicle (BEV) [5] variants of the Golf model series.

Vehicle Characteristic	VW Golf 1.0 TSI BMT	VW Golf (VII) e-Golf	Delta
Length	4258 mm	4270 mm	12 mm
Width	1799 mm	1799 mm	0 mm
Height	1492 mm	1482 mm	10 mm
Curb weight (with driver)	1026 kg	1615 kg	589 kg
Power	63 kW	100 kW	37 kW
Top speed	180 km/h	150 km/h	30 km/h
Range	1219 km	231 km	988 km
Energy consumption	4.1 L/100 km	12.7 kWh/100 km	-

The weight increase caused by a larger traction battery does not only affect vehicle consumption but also impacts other vehicle components. If a component becomes heavier or a new one is added during the development process, it leads to a primary weight change (PWC) [6] (p. 9). Using the above-cited example, the 127 kg of added battery weight is the PWC. A PWC, in turn, may require the resizing of other vehicle components. For example, to ensure the same driving performance, the drivetrain components must be adapted. The sum of the weight increases caused by this adaptation is the secondary weight change (SWC). On the other hand, the 78 L of battery increase represents the secondary volume change (SVC). Furthermore, the PWC, can also impact on further components, such as the wheels. A greater vehicle weight requires a greater tire volume and therefore new tire dimensions. The increase in tire volume can, in turn, impact on the available space at the front axle (SVC on the vehicle).

The modeling of vehicle weight in the early development design has already been researched by various authors. Yanni et al. [7], Mau et al. [8], and Felgenhauer et al. [9] present various empirical equations for vehicle weight estimation. However, these authors do not model SWC.

Alonso et al. [10] derive an empirical weight model by dividing the vehicle in modules and quantifying the SWC of each module. The results are further used to evaluate the effects of SWC on vehicle consumption. Nevertheless, the model considers only ICEVs.

Wiedemann et al. [11,12] develop a more detailed method for estimating BEVs weight. They derive a basis weight for the vehicle using the model of Yanni and further add to the basis weight the weight of the electric powertrain, which comprises traction battery, electric machine, power electronics, and transmission. The weight of these components is estimated by using empirical models. The Wiedemann model can estimate the SWCs, but only for the powertrain components.

Fuchs [6,13] creates a weight model for BEVs, dividing the vehicle into modules, which are, in turn, subdivided into their subcomponents. The weight of each subcomponent is modeled empirically or semi-physically. The method can estimate all SWCs.

Angerer et al. [14,15] and Del Pero et al. [16] focus on the influence of weight on BEVs consumption. Angerer uses the model of Fuchs to estimate the influence of weight fluctuations on vehicle dynamics and consumption. Del Pero and al. also focus on the effects of weight reduction on vehicle consumption. However, the model of Del Pero et al. simply consists of a longitudinal simulation and does not contain any weight modeling.

The above-cited authors mainly focus on the SWCs, without considering that a redesign of the components due to a PWC can trigger a change in the component volumes (i.e., a SVC). The SVC can further impact on the available installation space. This requires a check to ensure that the package of the vehicle remains feasible.

To our knowledge, no automatized method exists to simultaneously estimate both SWCs and SVCs. Thus, we aim to extend the existing SWC models with a package model that is capable of estimating the SVC triggered by PWC and SWC. With this method, it is possible, given a PWC, to do the following:

- Estimate the resulting SWCs;
- Estimate the SVC of the single components caused by the PWC and triggered SWCs;
- Estimate the SVC on the vehicle installation spaces caused by the components SVCs.

To show exemplary how this scope can be achieved, we present, in this paper, the developed model for the vehicle wheels. We focus on the wheels at the front axle, since it is the primary steering axle, and, therefore, the wheels greatly influence the available installation space for the powertrain components. Therefore, the SVCs triggered by the wheels are particularly relevant.

2. Materials and Methods

We subdivide the wheel into three subcomponents: brake discs (Section 2.2), rims (Section 2.3), and tires (Section 2.4). To describe these subcomponents (Figure 1), we employ empirical models, which require creating a components database (Section 2.1). After explaining how subcomponent models operate (Sections 2.2–2.4), we combine them to describe the entire wheel and conduct an evaluation of the wheel model (Section 3.1). This allows an estimation of SWCs and SVCs of the wheel, thus enabling a quantification of the SVC on the installation space at the front axle (Section 3.2).

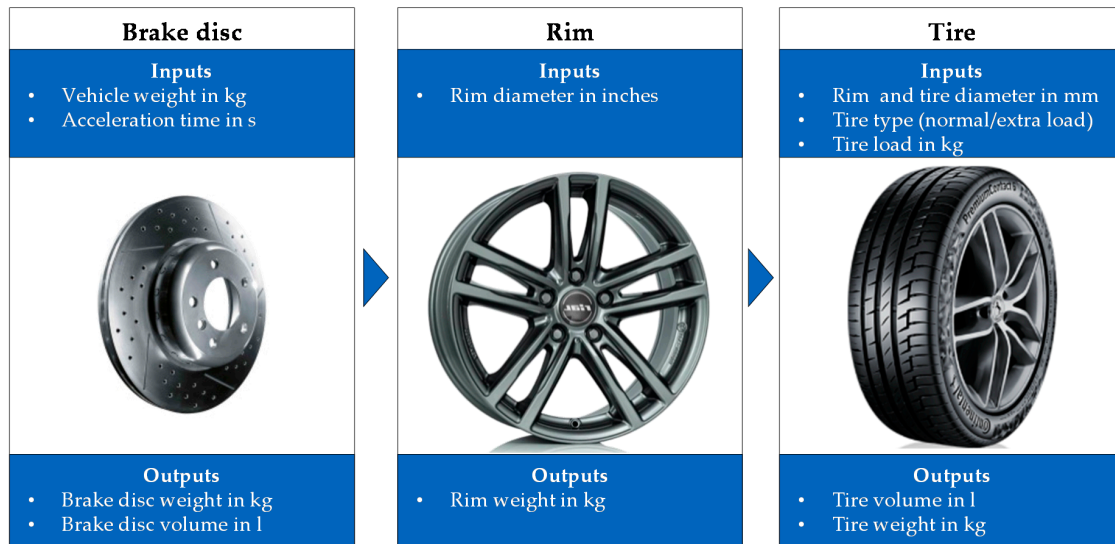


Figure 1. Overview of the subcomponent models, based on References [17,18].

2.1. Employed Databases and Methods

Due to the limited number of BEVs, it is necessary to include hybrid (HEVs) and plug-in hybrid vehicles (PHEVs) in the database. To ensure a homogeneous and up-to-date state of technology, we consider only vehicles built between 2010 and 2019.

To derive the parametric models for the wheel components, we employ two databases: A2Mac1 [19] and the catalog of the Allgemeine Deutsche Automobil-Club (ADAC) [20]. A2Mac1 is an automotive benchmarking service provider and offers precise and detailed component documentation for the vehicles of leading manufacturers. The ADAC is Europe’s largest automobile club [20], and its online catalog offers an extensive database with 96 current and discontinued brands and a complete list of their vehicles. The catalog assigns a map to each vehicle, which contains information on the overall vehicle level.

We use the A2Mac1 database to acquire data regarding the dimensions and weights of the wheel components. For the modeling of these components, a required variable is the vehicle weight. In this paper, we distinguish between vehicle curb weight (VCW) and vehicle gross weight (VGW). The difference between the two terms is explained below. In the automotive sector, the terms weight and vehicle weight are established definitions [6] (p. IV), which are used as synonyms for “mass”.

Therefore, in the scope of this paper, we employ the term weight when referring to the mass of the vehicle or one of its components.

A model series, for example, the Audi e-tron, contains different model variants: quattro, advanced quattro, and S line Quattro [21]. Each model variant has a different weight, which depends on its equipment. We dimension the brakes and tires so that they can withstand the weight of the heaviest model variant of the model series. This ensures that the dimensioned brakes and tires are compatible with all model variants within the model series. The vehicle models contained in A2Mac1 are not necessarily the heaviest variant of the model series, and therefore their VCW cannot be used to dimension the wheel's components. For this reason, we link each vehicle model of the A2Mac1 database with the corresponding ADAC model series. This step enables us to link the VCW of the corresponding heaviest model variant to each model documented in A2Mac1. An overview of the database can be found in Appendix A Tables A1–A3. In the next sections, when referring to the VCW, we mean the weight of the heaviest model variant of the model series in the vehicle empty state as defined by Reference [22].

Following §34 StVZO [23], the VGW is defined as the weight that must not be exceeded, considering the material stress, engine power, and emergency and long-lasting brake applications. The VGW is calculated from the sum of the VCW and the maximum vehicle payload, which depends on the equipment level and, therefore, on the model variant within a single model series. In this paper, when referring to the VGW, we mean the weight of the heaviest model variant of the model series.

The following subsections (Sections 2.2–2.5) describe the developed parametric models for estimating the volume and weight of the wheel components. The content of these subsections is required to understand the results presented in Section 3.

2.2. Brake Model

Two types of wheel brakes are used in passenger cars: drum and disc brakes [24] (p. 64). In today's vehicles, only front brakes are fitted with disc brakes, and drum brakes are used less often nowadays for rear-wheel brakes, which often use disc brakes instead [24] (p. 64). Therefore, in this paper, we will only focus on disc brakes.

BEVs, PHEVs, and HEVs can recuperate their kinetic energy during deceleration and store it in the traction battery [25]. During recuperation, the electric machine works like a generator: a deceleration of up to 0.3 g can be achieved without using the friction brakes [26]. Thus, most car journeys can be carried out without actuating the wheel brakes. This concept suggests the possibility of downsizing the brake system, which could reduce weight and costs [26]. However, for safety reasons, BEVs, PHEVs, and HEVs are tested for braking by using the same criteria as ICEVs [26]. Recuperation is completely disabled during the performance tests because, when the battery is fully charged or cold, the maximum regeneration potential is not available [27] (p. 29). The vehicle must always ensure maximum braking performance [26] under such conditions.

To provide long-range driving capability, BEVs are equipped with a large battery that can reach a considerable weight (in the case of the Audi e-tron, almost 700 kg [28]). As a result, BEVs are usually heavier than ICEVs with comparable exterior dimensions (see Table 1) [29] (p. 8). Moreover, HEVs and PHEVs are heavier than comparable ICEVs, due to the higher number of required components for the powertrain. Therefore, to comply with legal requirements, the brakes on these vehicles must be larger because the kinetic energy is higher compared to that of a similar ICEV traveling at the same speed [26] (p. 663). Thus, we do not include ICEVs in our database.

2.2.1. Volumetric Model

For the brake disc dimensions, we derive a linear regression model, which correlates the diameter of the brake disc (dependent variable) to the vehicle characteristics (independent variables). In order to identify the vehicle characteristics, which are suitable for modeling the brake disc dimensions, we must identify the central design focus for dimensioning this component.

To ensure safe driving, wheel brakes must be able to withstand heavy operating conditions. An important design criterion for braking systems is the thermal design. The thermal mass of the brake disc plays an important role in thermal stability: Larger and heavier brake discs have more heat-storage capacity and cooling properties. They are, therefore, better able to absorb the kinetic energy of the vehicle that is converted into heat during braking [30] (p. 72). The maximum value of the kinetic energy is calculated by considering the vehicle VGW $m_{veh\ max}$ and the maximum attainable speed $v_{veh\ max}$. The VGW and its top speed are, hence, suitable variables for estimating the brake disc diameter.

The thermal load of the brake discs is also determined by the time it takes to allow the brakes to cool down between two consecutive brake applications. This amount of time relates to the acceleration capability of the vehicle. The faster the vehicle can accelerate, the shorter the time available for brake cooling. This is particularly critical for cases like the AMS consumer test, which tests the braking performance of the vehicle [31]. For this reason, the acceleration time $t_{veh\ 0-100}$ from 0 to 100 km/h is a suitable vehicle characteristic for modeling the brake disc diameter.

We extract from A2Mac1 the brake disc diameter D_{brake} for the vehicles contained in Appendix A Tables A1–A3. The acceleration time and the VGW are obtained from the ADAC database. We correlate both variables to the brake disc diameter, thus deriving the linear regression model in Equation (1). A list of the symbols used in Equation (1) and the following equations can be found in Appendix A Table A4.

$$D_{brake} = 238.345\ \text{mm} + (0.053\ \text{mm/kg}) \times m_{veh\ max} - (5.631\ \text{mm/s}) \times t_{veh\ 0-100} \quad (1)$$

With this variable choice, we can model the thermal load of the vehicle, using the acceleration time, and the kinetic energy, using the VGW. For the modeling, we only consider ventilated discs, since all vehicles of the database mount ventilated discs as front brakes. The developed model achieves an R^2 of 87.3%, a mean absolute error (MAE) of 9.94 mm. The corresponding normalized mean absolute error (nMAE) is 3.22%.

2.2.2. Weight Model

The weight of a brake disc is mainly related to its diameter and its thickness. However, our statistical evaluation showed that the thickness is not a significant variable for weight modeling.

We extract the disc diameter and its weight m_{brake} for each of the vehicles in Appendix A Tables A1–A3. The resulting regression model describing the correlation between D_{brake} and m_{brake} is shown in Equation (2):

$$m_{brake} = -12.870\ \text{kg} + (0.069\ \text{kg/mm}) \times D_{brake} \quad (2)$$

The developed model achieves an R^2 of 91.33%, an MAE of 0.52 kg, and an nMAE of 6.42%.

We also model the weight of the brake calipers and brake pads. In both cases, it was not possible to set up a regression model to link the component's weight to the vehicle's characteristics; thus, we use constant values for the modeling. We extract for the vehicles in Appendix A Tables A1–A3 the weight values for the front brake calipers and the brake pads from A2Mac1. We derive a mean value of 5.46 kg for the brake calipers and a standard deviation equal to 1.70 kg. We derive a mean value of 1.02 kg and a standard deviation of 0.31 kg for the weight of each pair of front brake pads.

2.3. Rim Model

To model the rims, we use the nominal rim diameter, which is specified in inches by the manufacturer. It is not possible to create an empirical model, which estimates the rim diameter from dimensions of other components such as the tire diameter. Due to its importance as a design element, the rim and its dimensions do not depend exclusively on the tire diameter, but rather on the specific design strategy the manufacturer specifies. Therefore, we choose to use the rim diameter as the model input.

2.3.1. Minimum Rim Diameter

Since the rim diameter is an input for this model, we do not need to model the rim dimensions. Nevertheless, it must be guaranteed that the input rim diameter is compatible with the brake disc, i.e., that no collision occurs between the brake caliper and rim. To model this effect, we derive a minimum radial clearance, which must be maintained between brake and rim to avoid a collision.

The minimum radial clearance must be calculated, taking as reference the smallest rim offered in the model series, since this rim size represents the worst-case scenario. However, the vehicles documented in A2Mac1 are not necessarily the model variant with the smallest rim diameter. Therefore, we link each model variant of A2Mac1 with the corresponding model series in ADAC and extract from ADAC the smallest rim diameter offered inside the model series $D_{\text{rim min ADAC}}$. With these data, we calculate the minimum radial clearance $D_{\text{rim clearance}}$, as shown in Equation (3):

$$D_{\text{rim clearance}} = D_{\text{rim min ADAC}} - D_{\text{brake}} \quad (3)$$

We calculate the radial clearance for the vehicles in Appendix A Tables A1–A3 and derive a mean value of 122.24 mm, with a standard deviation of 27.25 mm.

2.3.2. Weight Model

To calculate the rim weight m_{rim} , we develop a regression model, which correlates m_{rim} with the rim diameter D_{rim} (expressed in inches). Equation (4) shows the resulting linear regression model:

$$m_{\text{rim}} = -13.063 \text{ kg} + (1.405 \text{ kg/inch}) \times D_{\text{rim}} \quad (4)$$

The model achieves an R^2 of 88.48%, an MAE of 0.64 kg, and an nMAE of 5.56%. Initially, we also tried to employ the rim material (aluminum or steel) as an independent variable, but it was categorized as statistically irrelevant. The same effect has also been observed by Fuchs [6] (p. 42).

2.4. Tire Model

The European Tire and Rim Technical Organization (ETRTO) defines a tire as a flexible element made of rubber and reinforcement materials [32] (p. G2). The significant tire parameters are the tire diameter, D_{tire} , the nominal aspect ratio, $h_{\%}$, and the section width, w_{tire} , which are described in the ETRTO manual [32] (pp. G2–G13). In this paper, when referring to the tire diameter, we mean the outer diameter of the wheel. The tires have a great impact on vehicle design [33], and their diameter also depends on the design strategy of the individual manufacturer. Thus, we decide to implement the tire diameter as model input.

2.4.1. Volumetric Model

The volumetric model is implemented as follows: First, the axle load is calculated, thus deriving the required tire load capacity. Subsequently, the tire volume is estimated, empirically, according to the required tire load capacity. Finally, using the rim diameter and tire diameter inputs, the empirically estimated volume is corrected, and the further tire dimensions' section width and aspect ratio are derived. The exact implementation of these steps is explained below.

The tire volume, V_{tire} , is defined as the volume of gas contained between the rim and tire under pressure. Given the tire diameter, the corresponding volume can be calculated by using Equation (5):

$$V_{\text{tire}} = 0.25 \times \pi \times w_{\text{tire}} \times (D_{\text{tire}}^2 - D_{\text{rim}}^2) \quad (5)$$

To dimension the tire, engineers select the appropriate section width and aspect ratio, which can provide the air volume needed to support the VGW and is compatible with the desired rim diameter. Wider tires provide better traction when accelerating: A large contact area helps powerful vehicles

reduce tire slippage when accelerating from standstill and improve acceleration time. Therefore, we set minimal values for the tire width, depending on the vehicle's power and drivetrain (front-wheel drive, rear-wheel drive, or all-wheel drive) according to Reference [34] (p. 22).

The required tire volume depends on the required tire load capacity, which is the maximum load a tire can carry under specified conditions of use [32] (p. G5) and is coded by the load index. Depending on the structure of the tire, we need to distinguish between standard and extra-load tires. Tires with the additional "extra-load" marking are designed for loads and inflation pressures higher than the standard version [32] (p. G10).

The required tire load capacity depends on the load at the axle. To calculate the axle load and to select the appropriate tire dimensions, the ETRTO manual defines two loading conditions: the 88% rule and the 100% rule [32] (pp. P15–P17). The manual further prescribes for each loading condition the number of passengers aboard and the load stowed in the luggage compartment. Starting with the VCW, the vehicle must be loaded with the prescribed number of passengers and luggage load, thus yielding the loaded weight for the 88% rule ($m_{88\%}$), and the loaded weight for the 100% rule ($m_{100\%}$).

By applying the described loading conditions and knowing the positions of the rows of seats, the position of the luggage compartment, and the axle load distribution of the empty vehicle, it is possible to compute the new axle distribution according to the 100% and 88% rules. We can then derive the distances $l_{F,88\%}$ and $l_{F,100\%}$ between the center of mass and the front axle for both load cases. Finally, by using l to denote the vehicle wheelbase, we can calculate the tire load (in kg) according to the 88% rule, using Equation (6):

$$L_{\text{tire}88\%} = (m_{88\%} \times (l - l_{F,88\%})) / (2 \times l \times 0.88) \quad (6)$$

Using the same method, we calculate the tire load for the 100% rule (Equation (7)):

$$L_{\text{tire}100\%} = (m_{100\%} \times (l - l_{F,100\%})) / (2 \times l) \quad (7)$$

For the following tire dimensioning, we consider the loading condition, which generates the highest tire load. We then derive a regression that correlates the required tire volume (dependent variable) to the occurring tire load (independent variable). The data needed for this purpose are collected from the ETRTO manual [32]. The ETRTO lists for every tire contained in the manual the corresponding volume and the maximum tire load capacity (in kg), which allows us to set up calculate a regression linking these two variables. For the modeling, we consider all the standard- and extra-load tires listed in the manual section "Passenger car tires". The tire volume, V_{tireSL} , allowing a standard-load tire to carry a given load, L_{tire} (in kg), is defined by Equation (8):

$$V_{\text{tireSL}} = -13462233.892 \text{ mm}^3 + (87651.102 \text{ mm}^3/\text{kg}) \times L_{\text{tire}} \quad (8)$$

The developed model achieves an R^2 of 98.68% and an nMAE of 2.83%. For extra-load tires, the tire volume is calculated according to Equation (9). The developed model achieves an R^2 of 98.82% and an nMAE of 2.63%:

$$V_{\text{tireEL}} = -13548645.429 \text{ mm}^3 + (77990.623 \text{ mm}^3/\text{kg}) \times L_{\text{tire}} \quad (9)$$

The main drawback of the empirical models in Equations (8) and (9) is that, although they estimate a minimum required tire volume, they do not ensure that the resulting volume is realistic. In fact, the tire volume cannot assume arbitrary values, since the tire dimensions have specific proportions regarding section width and nominal aspect ratio, which are documented in the ETRTO manual. Regarding the tire section width, the manual prescribes values ranging between 125 and 355 mm. The tire section width is always expressed as a multiple of five but not ten, with an interval of 10 mm between two consecutive values. For the nominal aspect ratio, the manual prescribes values between 25% and 80%. The aspect ratio is always expressed as a multiple of five with an interval of 5% between

two consecutive values. Therefore, the tire volumes resulting from the regression models have to be corrected to ensure that the volume can be generated from admissible values of tire width and aspect ratio. Figure 2 shows the correction method, which is divided into three steps.

In the first step (Figure 2), we combine the input rim diameter, D_{rim} (in mm), with every possible nominal aspect ratio and section width combination and derive the tire diameter, as shown in Equation (10):

$$D_{tire} = D_{rim} + (2 \times w_{tire} \times h_{\%})/100 \tag{10}$$

The result is a tire diameter matrix (Figure 2) containing all the possible diameters that are compatible with the input rim size. From this matrix, we use Equation (5) to derive the matrix for the corresponding volumes (volume matrix, Figure 2).

In the second step (Figure 2), the diameter and volume matrices are compared with the input tire diameter and the minimum tire volume from Equations (8) and (9). Based on this comparison, we generate two matrices that describe the percentual deviation from the single elements of the diameter matrix or volume matrix to the input tire diameter or minimum tire volume.

Finally, in the third step (Figure 2), we choose from the two deviation matrices the tire that has the smallest deviation from the calculated volume and the desired diameter. This results in the final values for the tire diameter and volume, as well as the aspect ratio and width. After this step, the dimensions of the tire are fully defined.

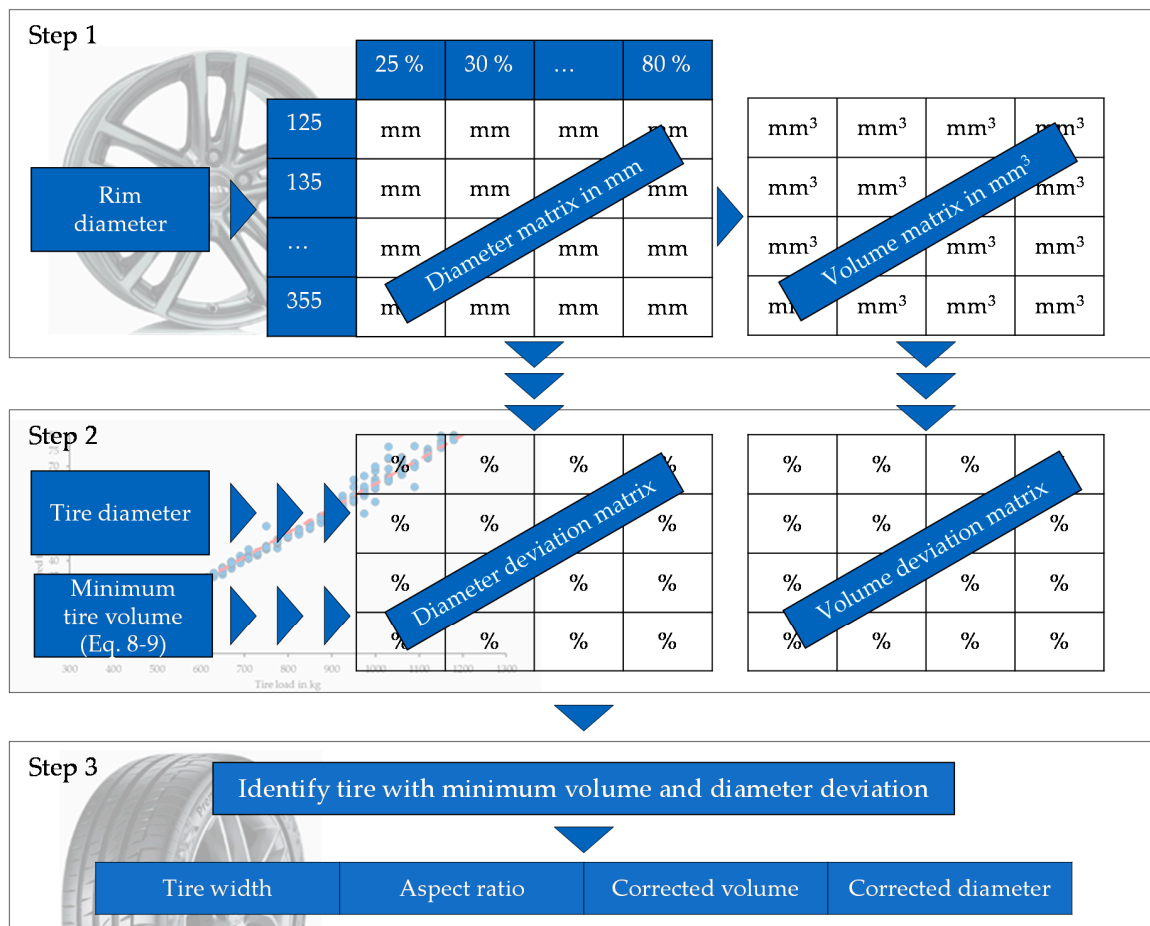


Figure 2. Overview of the correction method for the tire dimensions.

2.4.2. Weight Model

For the weight analysis, we implement a regression model that estimates the tire weight, m_{tire} , based on the tire diameter and its section width. The regression is derived from the evaluation of the vehicles in Appendix A Tables A1–A3 and shown in Equation (11):

$$m_{\text{tire}} = -16.890 \text{ kg} + (0.023 \text{ kg/mm}) \times D_{\text{tire}} + (0.054 \text{ kg/mm}) \times w_{\text{tire}} \quad (11)$$

The developed model has an adjusted R^2 of 85.85%, an MAE of 0.71 kg, and an nMAE of 6.63%.

2.5. Wheelhouse Model

Given the tire dimensions, we can estimate the wheelhouse dimensions. In this paper, we focus on the wheelhouse width, $w_{\text{wheelhouse}}$. Given the wheelhouse width, the position of the side roll rail can be identified. Then, knowing the vehicle width at the front axle (W_{106}) and the width of the side roll rail w_{srr} , we estimate the available space at the front axle, $w_{\text{available}}$, as shown in Equation (12):

$$w_{\text{available}} = (W_{106} - 2 \times w_{\text{wheelhouse}} + w_{\text{srr}}) \quad (12)$$

In the further steps of the product specification, $w_{\text{available}}$ can be compared with the actual space required by the powertrain components, w_{required} , to test the vehicle concept feasibility. Figure 3 illustrates the above-cited measures.

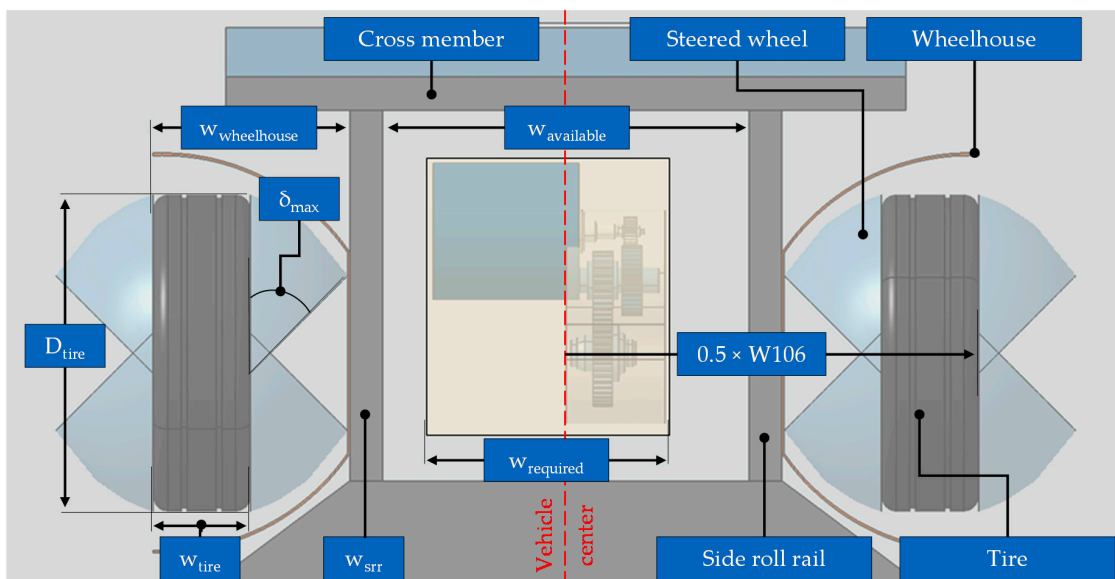


Figure 3. Overview of the relevant measures at the front end of the vehicle, based on Reference [3].

In the later sections, we consider the w_{srr} as constant, since our focus is on the wheelhouse dimensions. A change in the wheel dimensions leads to a variation of $w_{\text{wheelhouse}}$, which depends on the tire diameter, the tire section width, and the maximum wheel steering angle, δ_{max} . If we simplify the model by assuming that the wheel steers at its center (located at the half of the tire width), the wheelhouse width can be derived according to Equation (13):

$$w_{\text{wheelhouse}} = 0.5 \times w_{\text{tire}} \times \cos \delta_{\text{max}} + 0.5 \times D_{\text{tire}} \times \sin \delta_{\text{max}} + 0.5 \times w_{\text{tire}} \quad (13)$$

The δ_{max} is usually reached when driving slowly or during parking. For this scenario, we assume an Ackermann characteristic for the steering [35] (pp. 379–380). The inner wheel steering angle is always bigger than that of the outer wheel and thus determines the width of the wheelhouse. Therefore,

in Equation (14), we can estimate the δ_{\max} from the vehicle turning radius (R_{turning}), wheelbase (L101), front overhang (L104), maximum width (W103), and track width (W101):

$$\delta_{\max} = \text{atan}(L101/(-W103 \times 0.5 + (R_{\text{turning}}^2 - (L101 + L104)^2)^{0.5} - W101 \times 0.5)) \quad (14)$$

By combining the result of Equation (14) with the wheel dimensions (Section 2.4), it is possible to estimate the wheelhouse width using Equation (13).

3. Model Evaluation and Results

In the first part of this section, we carry out an evaluation based on a vehicle database, to assess the accuracy of the wheel model. In the second section, we apply a parameter variation to the model in order to quantify the SWC on the wheel and SVC on the wheel and on the vehicle.

3.1. Model Evaluation

To model the SVCs, the accuracy of the estimation of the tire volume and the tire width must be tested. To reach this scope, we first need to create an evaluation database.

We set up the evaluation database, using A2Mac1, ADAC, and the ETRTO manual. We extract from the A2Mac1 database the following information: vehicle axle distribution, the position of the rows of seats, position of the luggage compartment, and the tire load index. The ETRTO manual lists every available tire dimension and the related load indexes. Therefore, using the load indexes, we link the A2Mac1 database with the ETRTO manual, thus identifying which model variants of the A2Mac1 database mount a standard and which an extra load tire. We further link the A2Mac1 models with the corresponding model series in ADAC, thus identifying the VCW of the heaviest model variant for each A2Mac1 model and the exact dimensions of the tires. It was not possible to conduct the above-cited linking for all the vehicles of Appendix A Tables A1–A3 because some information was missing for some vehicles, or no ADAC model series could be found. Appendix A Table A5 shows an overview of the evaluation database.

To evaluate the tire volume model, we assign as inputs the vehicle empty axle load, the tire diameter, the rim diameter, the vehicle's outer dimensions, the VCW, and the vehicle payload. With these inputs, we calculate the VGW for each vehicle of the database. We then calculate the tire load as in Equations (6) and (7), using the positions of the row of seats and the luggage compartment. We suppose that the axle distribution for the heaviest model variant corresponds to the axle distribution given in A2Mac1. Subsequently, we estimate the required tire volume according to the mounted tire type, using Equations (8) and (9). Finally, we conduct the correction method shown in Figure 2. The results are presented in Figure 4.

The X-axis in Figure 4 presents the tire volume resulting from the model, and the Y-axis shows the real tire volume. The resulting estimation has an R^2 of 91.0%. For most of the vehicles, the volume is slightly underestimated. This depends on the fact that the different manufacturers use safety factors, dimensioning the tire by using loads, which are higher than the real load. With this strategy, it is possible to compensate for weight estimation errors that can occur in the later specification phase. The volume is overestimated for the BMW 5-Series, the Jaguar I-Pace, and the Kia Niro. Regarding the BMW and the Kia, the error can be attributed to slightly inaccurate load-distribution data, which lead to an overestimation of the required tire volume. The reason for overestimating the Jaguar is explained in the tire-model-width-evaluation section.

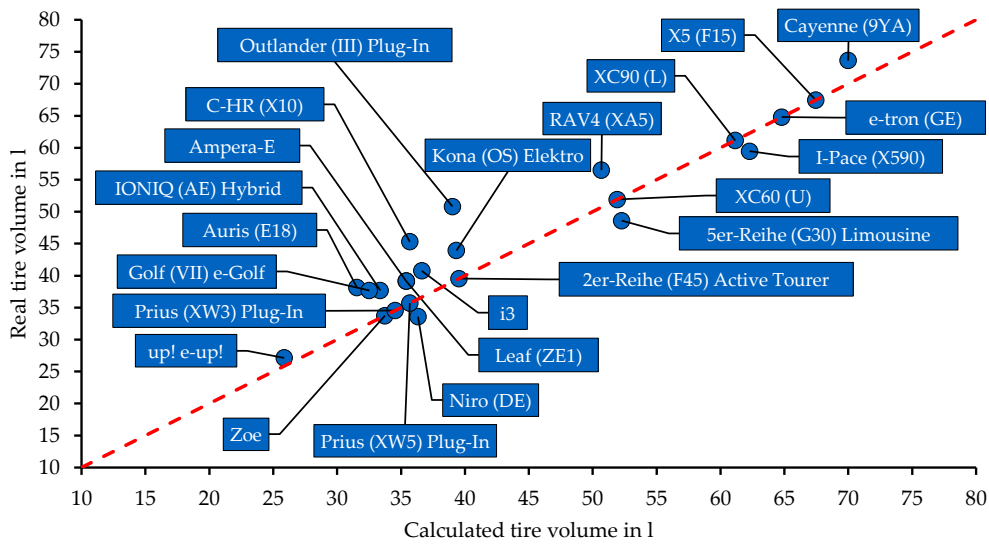


Figure 4. Whole-model plot for the tire-volume evaluation.

We use the same database to evaluate the precision of the tire width estimation. Our wheel model calculates the tire dimensions that fulfill the conditions given on the required tire diameter, the calculated tire volume, and the desired rim diameter, according to the method described in Section 2.4.1. The tire width is calculated for each vehicle listed in Appendix A Table A5 and compared with the real values (Figure 5). The tire width model achieves a R^2 of 77.0%. The tire width is overestimated for the BMW 5-er (G30), the Jaguar I-Pace (X590), and the Kia Niro (DE). The slightly overestimated tire volume leads to an overestimated tire width for the BMW and the Kia. The required tire volume would be estimated correctly for the Jaguar; however, the calculated value for the tire width of 265 mm is higher than the real one (245 mm). This result is caused by the constraint on the minimal tire width, which is set equal to 255 mm due to the high power of this car’s drivetrain. For the same reason, the resulting volume is also overestimated.

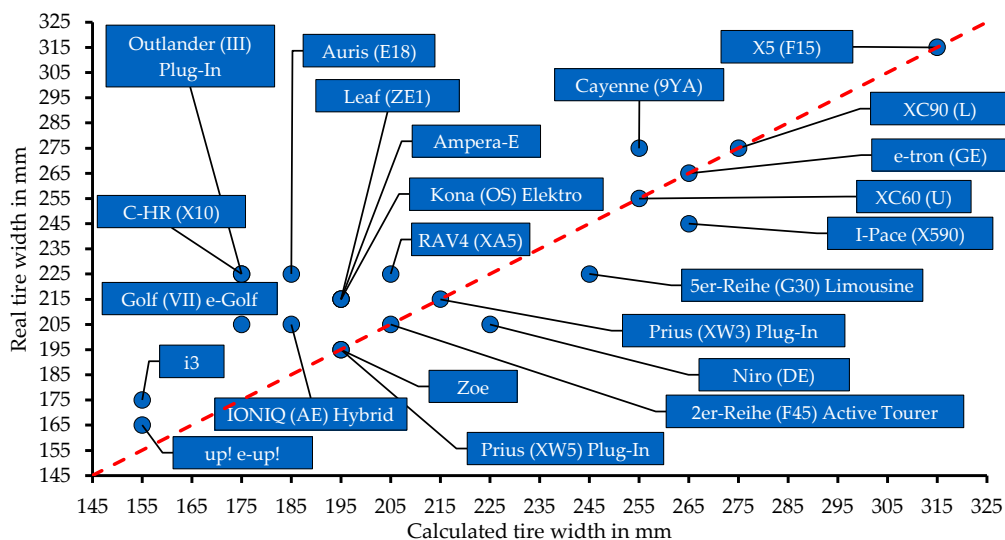


Figure 5. Whole-model plot for the tire-width evaluation.

Another cause of deviations from the real tire width values is that our model calculates the tire dimensions only in dependency on the vehicle weight and power without considering lateral dynamic requirements. We do not have enough data to model the lateral dynamic requirements; therefore, we cannot consider this influence.

3.2. Quantification of the Secondary Effects on the Wheel Components

In this section, we apply the wheel model to four reference vehicles, each belonging to a different segment. We intend to evaluate the SVCs and SWCs resulting from a stepwise increase in the VCW, which is denoted in the following sections as the PWC. The reference vehicles are shown in Table 2; the data are collected from the ADAC catalog. Table 2 shows the initial VCW and the tire and rim diameter, which are simulated. The further vehicle data required for implementing Equations (12) to (14) are collected from the A2Mac1 database and are not shown in the table.

Table 2. Reference vehicles used for analyzing secondary effects on the wheel components.

Vehicle Model (Model Series)	Initial VCW	Min–Max Diameter Rim Variants	Mean Outer Tire Diameter
Renault Zoe 22 kWh (Zoe (06/13-09/19))	1547 kg	16"–17"	621 mm
Nissan Leaf 40 kWh (Leaf (ZE1) (from 01/18))	1580 kg	16"–17"	640 mm
Audi e-tron 55 quattro (e-tron (GE) (from 03/19))	2565 kg	19"–21"	765 mm
Jaguar I-Pace (I-Pace (X590) (from 10/18))	2208 kg	18"–22"	759 mm

VCW = vehicle curb weight.

Regarding the tire diameter, it can vary of a few mm inside a model series, depending on the chosen rim. For the simulation, we take for each reference vehicle the mean value of all the offered tire diameter of the corresponding model series. Therefore, our method dimension the tire so that the resulting diameter is as close as possible to the diameter shown in Table 2.

In our analysis, we dimension the tires considering the maximum rim size inside of the model series (Table 2). If the diameter is kept constant, a bigger rim reduces the tire sidewall and requires a wider tire to fulfill the volume requirement. Furthermore, the wheel equipped with the biggest rim is the heaviest wheel variant. Therefore, focusing on the maximum rim size allows us to consider the worst-case scenario for both volume and weight analysis. Nevertheless, the minimum rim size cannot be ignored, since the more the PWC increases, the bigger the brake disc diameter becomes, which could cause incompatibility between the minimum rim size and the brake disc. We discuss this subject in the next section.

We do not consider the limitation on the minimal tire width, due to the vehicle's power (Section 2.4.1), in order to highlight the effects of the weight increase alone.

We subdivide the quantification of the secondary effects in four steps. In the first step (Section 3.2.1), we analyze the influence of the PWC on the wheel volume, thus quantifying the SVC of the wheel. In the second step (Section 3.2.2), we quantify the influence of the PWC on the wheel, thus estimating the SWC. In the third step (Section 3.2.3), we combine the SVC of the wheel with the wheelhouse model (Section 2.5) and the dimensional chain presented in Equation (12) and Figure 3. This allows an estimation of the SVC on the $w_{\text{available}}$ (Section 2.5). Finally, in the last step (Section 3.2.4), we invert Equation (12) to simulate a strategy, where the SVC of the wheel is compensated by increasing the vehicle width.

3.2.1. Influence on the Wheel Volume (SVC on Component Level)

An increased PWC leads to a greater tire load, which requires a redesign of the tire, thus affecting its volume (Figure 6). The X-axis in Figure 6 represents the PWC (in %) with respect to the initial VCW. For example, for the Audi e-tron, a PWC of 5% with respect to the initial VCW of 2565 kg (see Table 2) corresponds to a weight increase of approximately 128 kg. The steps in Figure 6 represent the points where the PWC requires a redesign of the tire, i.e., causes a SVC.

As the model also dimensions the brake disc sizes (Section 2.2.1), we can test if the smallest rim size offered for the vehicles of Table 2 has enough radial clearance from the brake disc. This is particularly interesting for the case of the Audi e-tron. The increment of the brake disc diameter caused by a PWC of approximately 0.7% (corresponding to a VCW increase of 17 kg) causes an incompatibility with the given minimum rim size of 19", as the minimum radial clearance (see Equation (3)) is not fulfilled. To overcome this problem, we distinguish between two possible strategies.

In the first strategy (Audi e-tron 55, two rim variants), the rim size of 19" is simply excluded from the model series, which means that the customer can configure the vehicle with only two rim sizes (20" and 21"). With this strategy, the minimum rim size changes to 20", thus avoiding the collision between the brake disc and rim. The tire volume does not have to be changed until a PWC of around 8% (Figure 6). The maximum rim size remains unchanged (21").

In the second strategy (Audi e-tron 55, three rim variants), we impose the requirement that, despite the unfulfilled radial clearance, the vehicle must be configurable by using three rim variants. Such a strategy could be imposed for design reasons or to offer a high product range to the customer. Therefore, since the 19" rim is incompatible with the brake disc after a PWC of 0.7%, it is necessary to start from a minimum rim of 20" and also offer the variants 21" and 22", shifting the maximum rim size from 21" to 22". Increasing the maximum rim diameter leads to a decrease in tire volume (because the tire diameter remains constant), which requires a change of the tire section width and nominal aspect ratio in order to comply with the minimum volume requirement. In this particular case, it is possible to find a section width and aspect ratio combination that comes closer to the minimum required volume than the previous one, which explains the slight volume reduction at 0.7% (Figure 6). Nevertheless, this tire combination has a greater section width than the initial one. The effects caused by this redesign are shown in Section 3.2.3.

Regarding the other vehicles, the same effect as the Audi e-tron occurs also for the Nissan Leaf at a PWC of around 6.5% (corresponding to a weight increase of 102 kg). For the sake of simplicity, we do not distinguish between two cases for this vehicle and suppose that a strategy corresponding to the "Audi e-tron 55, three rim variants" is applied, i.e., the number of offered rim variant does not change.

The remaining volume changes, such as the step at 5.2% for the Renault Zoe or the step at 5.8% for the Jaguar I-Pace, are caused by an increase of the tire section width, which is required to compensate for the increase of the minimum required tire volume.

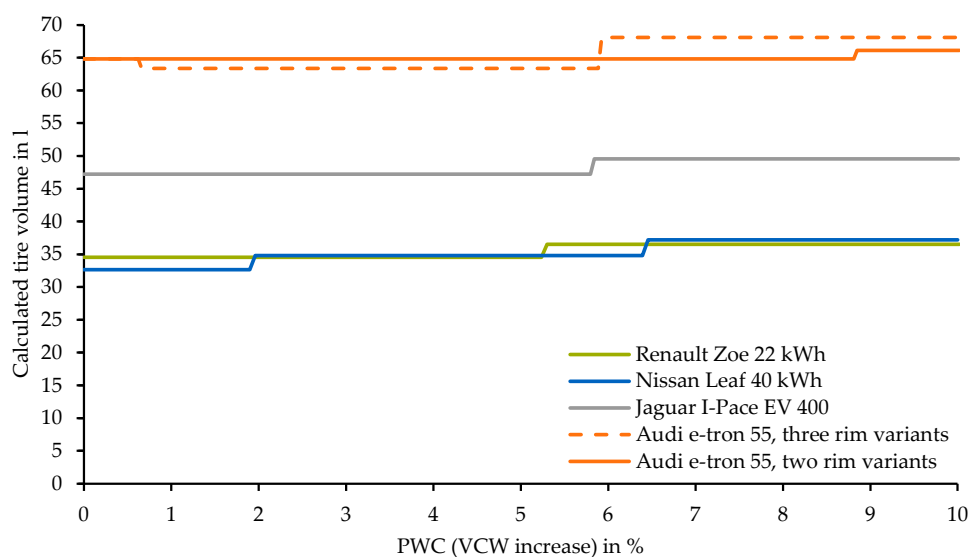


Figure 6. Interdependency between secondary volume change (SVC) of the wheel and the primary weight change (PWC).

3.2.2. Influence on the Wheel Weight (SWC on Component Level)

For each PWC, we recalculate the dimensions of the brake disc (Section 2.2.1), rim (Section 2.3.1), and tire (Section 2.4.1). The hereby calculated dimensions can be further employed for the weight models of Section 2.2.2, Section 2.3.2, and Section 2.4.2, thus allowing an estimation of the total wheel weight. Figure 7 shows the SWC of the wheel caused by the PWC.

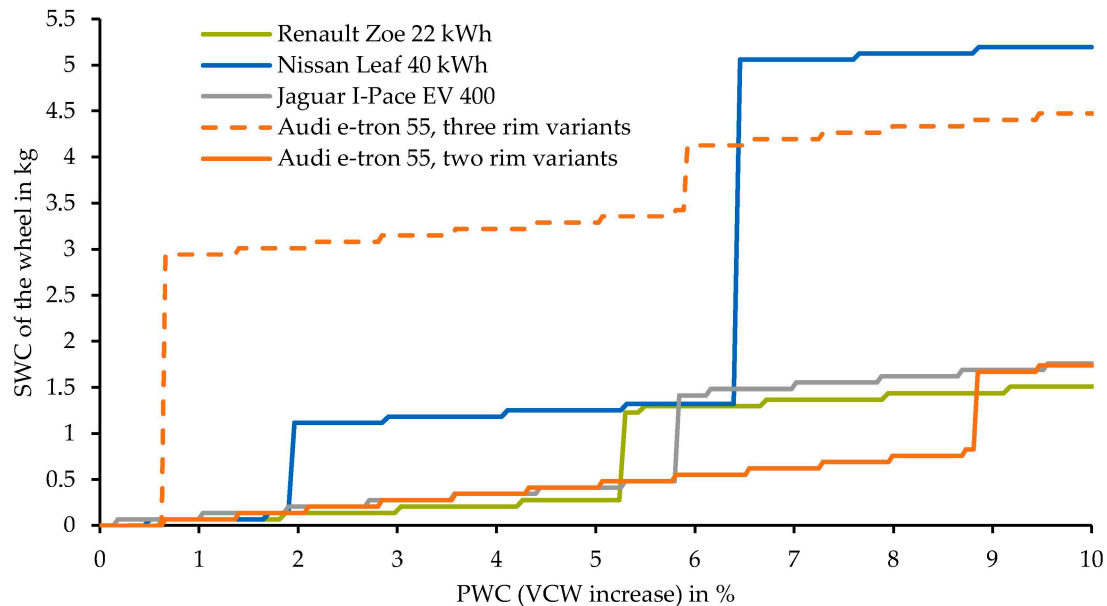


Figure 7. Interdependency between SWC of the wheel and PWC.

The small steps are related to an increase of the brake disc diameter, while the bigger ones are caused by an increase of the tire width. The great SWC at 0.7% for the strategy “Audi e-tron three rim variants” results from the change in the maximum rim size needed to offer the same number of rim variants: Both the weights of tire and rim change significantly. Figure 7 shows how limiting the maximum rim diameter on the Audi e-tron to 21” allows a wheel weight reduction of approximately 3 kg (for a VCW increase of 6%) with respect to the 22” variant. Reducing the number of rim variants from two to one would also avoid the step at 6.5% for the Nissan Leaf.

In conclusion, if we do not consider the cases of the Audi e-tron and the Nissan Leaf, where the rim size must be changed, we can conclude that the SWC caused by a PWC of 6% is comprised in a range between 0.5 and 1.5 kg per wheel. If we further assume that the vehicles mount the same wheel components at the front and rear axles, this corresponds to a total SWC between 2 and 6 kg.

3.2.3. Influence on the $w_{\text{available}}$ (SVC on Vehicle Level)

The outer tire diameter is an input of the model and remains constant regardless of PWC. The maximum rim diameter also remains constant as long as no collision between the brake disc and base rim occurs. Therefore, to compensate for the volume increase shown in Section 3.2.1, the tire must necessarily become wider. A change in the tire dimensions leads to a variation of the wheelhouse width as shown in Section 2.5 and Equation (13). Figure 8 shows the increase of wheelhouse width in mm, using the initial wheelhouse width as reference.

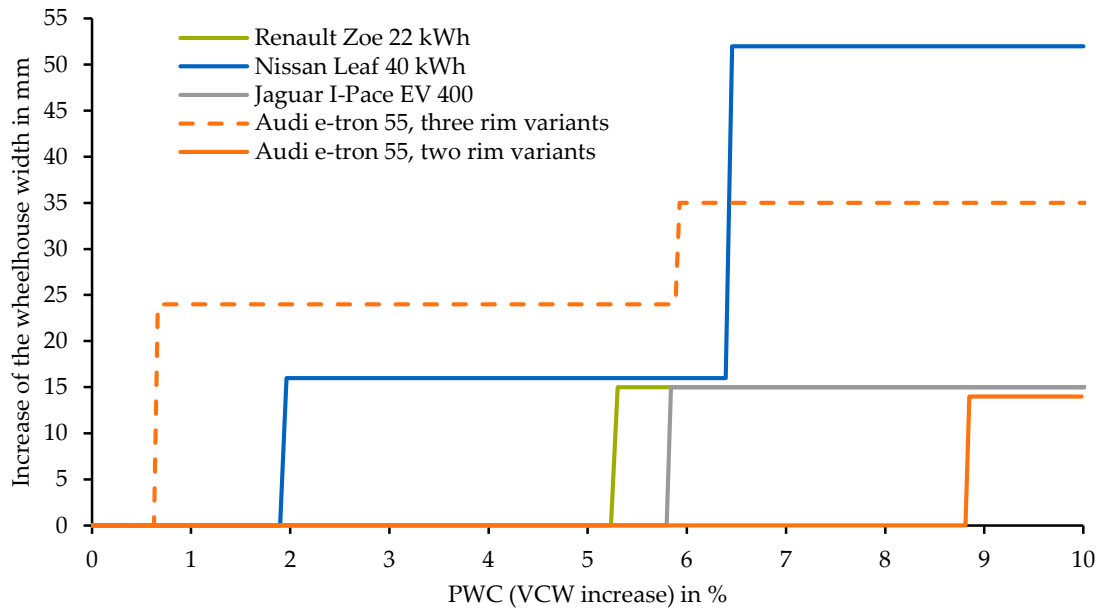


Figure 8. Interdependency between wheelhouse width and PWC.

Finally, using the results shown in Figure 8, we evaluate the variation of $w_{available}$ caused by the PWC. We apply to the four vehicles the dimensional chain depicted in Equation (12). For this calculation, we only model the wheelhouse width variation caused by the PWC, while keeping the values W_{106} and w_{srr} constant. Figure 9 shows the loss, in percentage, of $w_{available}$, using the initial $w_{available}$ as reference.

For the reference vehicles, a PWC of approximately 6% leads to a loss in $w_{available}$ of up to 12%. Regarding the Nissan Leaf, it is clearly shown that keeping the same number of rim variants is not a good strategy, since it can lead to a loss in $w_{available}$ greater than 10%. Limiting the Audi e-tron number of rim variants to two can avoid loss of approximately 6% at the front end (for a PWC above 8%).

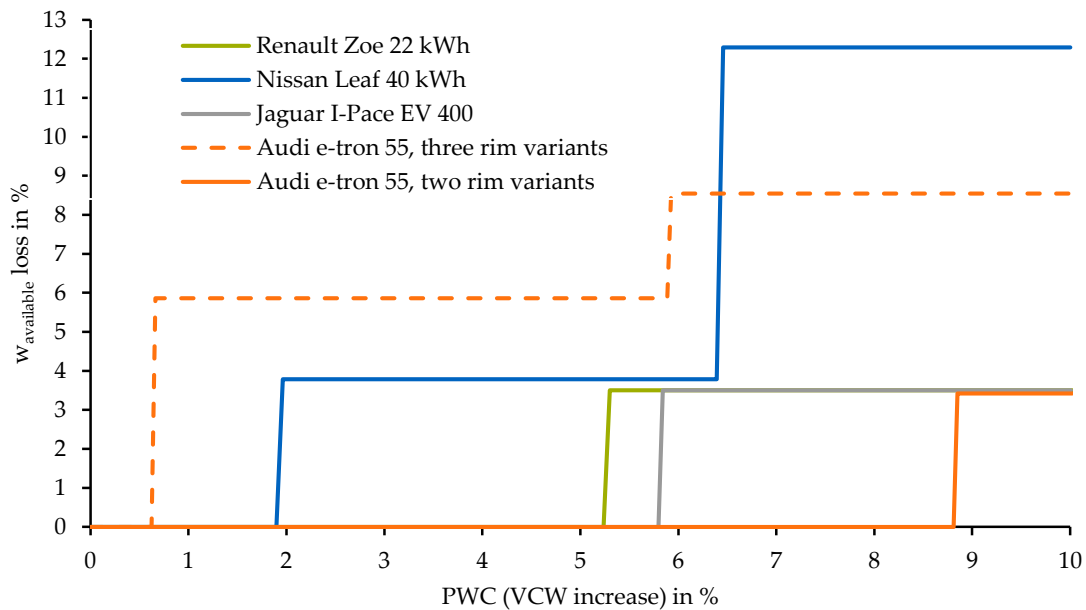


Figure 9. Interdependency between the SVC at vehicle front end and the PWC.

3.2.4. Influence on the Vehicle Outer Dimensions (SVC on Vehicle Level)

As shown in the previous section, the PWC greatly influences the $w_{\text{available}}$. The size of the powertrain components can be only roughly estimated due to the lack of known design parameters during early development design. Therefore, it is advisable to reserve some extra space for these components, thus enabling more freedom in the later course of the development.

For this reason, if the manufacturer does not want to accept a loss of $w_{\text{available}}$, another possibility is to increase the vehicle width. While inverting the dimensional chain shown in Equation (12), the increase in wheelhouse width (Section 3.2.2) can be compensated by increasing vehicle width (W106). This inevitably increases the vehicle outer dimensions (Figure 10).

Although this strategy counters the SVC of the wheel, it has a major drawback. The increase in the vehicle outer dimensions directly impacts the VCW. This can be shown by using the empirical model presented by Fuchs [6] (p. 40) for estimating the weight of the body in white (BIW). The BIW weight, m_{BIW} , can be modeled from the vehicle volume, V_{veh} , as presented in Equation (15) [6] (p. 40):

$$m_{\text{BIW}} = (37.45 \text{ kg/m}^3) \times V_{\text{veh}} - 66.38 \text{ kg} \quad (15)$$

To model the V_{veh} , Fuchs distinguishes among different body frames. For example, for the “hatchback” body frame, the volume can be modeled by using the vehicle width (W103), the front and rear overhangs (L104, and L105), the vehicle height (H100), and its wheelbase (L101) as in Equation (16) [6] (p. 39):

$$V_{\text{veh}} = (0.5 \times L104 + 0.75 \times L105 + L101) \times W103 \times H100 \quad (16)$$

It can be seen that a percentual increase in the W103 causes the same percentual increase in the V_{veh} , thus influencing m_{BIW} . By applying the model for the three rim variants of the Audi e-tron, a 4% increase of the W106 would correspond to a VCW increase of 20 kg based solely on the BIW.

In conclusion, although this strategy avoids a loss of $w_{\text{available}}$, it also causes further SVC in other parts of the vehicle. These SVCs can, in turn, cause additional SVCs.

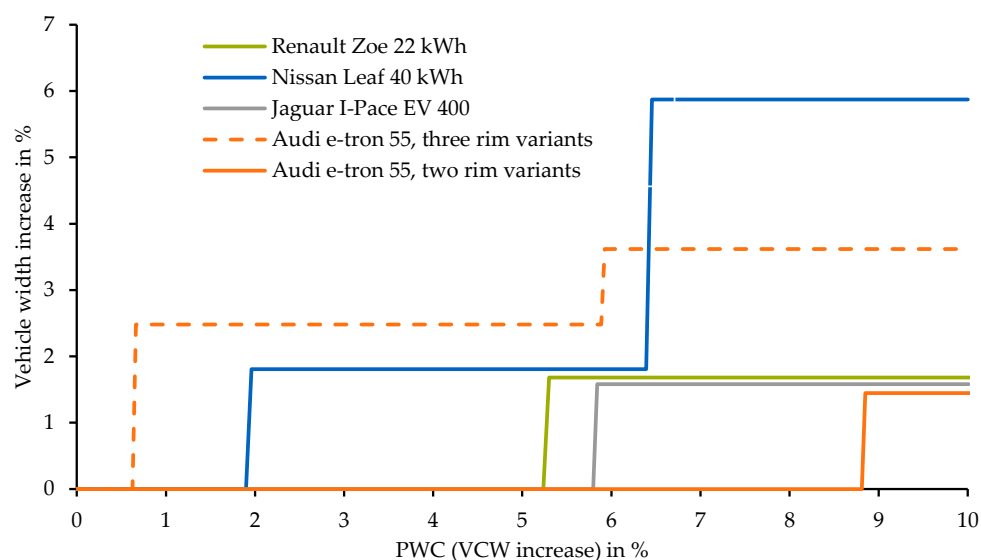


Figure 10. Interdependency between the vehicle width and the PWC.

4. Discussion and Conclusions

The presented model enables us to quantify the SVC and SVC of the wheels and to further model the triggered SVC at the front end of the vehicle. It further allows us to estimate the effects of various design strategies.

After introducing the subcomponent models (Section 2.2, Section 2.3, Section 2.4 and Section 2.5), we combine them to create a complete wheel model and further evaluate it (Section 3.1). For the subcomponent models, such as brake disc weight and dimensions, no evaluation is required, since the performance of the model is already described by the R^2 , nMAE, and MAE, which are listed in the corresponding model section. Regarding the evaluation of the wheel volume and width, the deviations from the real values mainly depend on the employed tolerances from the manufacturers, which we are not able to estimate. Additional errors may also be caused by the fact that we do not know the exact position of the center of gravity (and therefore the axle distribution) of the heaviest model variant, and we have to suppose that it corresponds to the distribution of the model variant given in A2Mac1.

The model shows that, depending on the vehicle and the applied design strategy, the SWC on the wheels is contained in a range between 2 and 6 kg. If the design strategy is poorly chosen, the SWC can increase up to 20 kg (as in the case we simulated for the Nissan Leaf). These SWC are still too low to trigger further SVCs. Nevertheless, it must be considered that the wheels are not the only components that are affected by SWCs. The same tendency will be observable for components such as the electric machine, body in white, axles, and, most importantly, the traction battery. The sum of the SWCs of these components can, in turn, cause further SWCs [10] and SVCs. Furthermore, an increase in the wheel weight impacts on its inertia, which can lead to higher vehicle consumption. This, in turn, can require a higher battery capacity and generate further SWCs. These effects can be only modeled by coupling the weight model with a longitudinal dynamic simulation. This topic will be addressed in further publications.

While the SWC is relatively low, the SVC on the vehicle shows great relevance. A PWC corresponding to 6% of the initial VCW can cause a loss in $w_{\text{available}}$ of up to 12%, depending on the applied strategy and on the vehicle characteristics. These results highlight the importance of a SVC estimation in early development, most of all for BEV, which are particularly subject to weight fluctuations. The SVC on the vehicle is highly dependent on the vehicle segment, the design strategy, and the VCW. Nevertheless, the presented methodology is capable of taking into account all of these effects and can be employed to identify SVC already in the early development phase. The approach is developed by following the actual dimensioning methods used by the manufacturers, which enable integration in the manufacturer developing process and can thus minimize the errors and reduce the number of iterations and costs.

In conclusion, in this paper, we quantify the SVC and SWC caused by the wheels and propose an effective approach for addressing the problems they cause. In future publications, we will apply the presented method to further vehicle components, thus expanding the SWC estimation to all the relevant vehicle components. This will allow precise modeling of SWCs and SVCs on other vehicle areas, such as the rear end and the installation space for the battery.

Author Contributions: As first author, L.N. defined the approach for the development of the presented model, identified the relevant components, and detailed the method and the data evaluation. A.R. supported during his semester thesis with the creation of the database, the derivation of the regression models, and the evaluation. A.K. and F.S. supported by the definition of the concept and proofread the paper. M.L. made an essential contribution to the conception of the research project. He revised the paper critically for important intellectual content. M.L. gave final approval of the version to be published and agrees to all aspects of the work. As a guarantor, he accepts responsibility for the overall integrity of the paper. All authors have read and agreed to the published version of the manuscript.

Funding: The research of L.N. was funded by the AUDI AG and the Technical University of Munich. The research of A.K. and F.S. is accomplished within the project "UNICARagil" (FKZ 16EMO0288). A.K. and F.S. acknowledge the financial support for the project by the Federal Ministry of Education and Research of Germany (BMBF).

Acknowledgments: The author L.N. would like to thank the colleagues of the AUDI AG in the persons of Maximilian Heinrich, Martin Arbesmeier, and Alois Stauber, who provided support during concept development. The authors would like to thank A2Mac1 EURL, in the person of Pir Ivedi, for the access to the A2Mac1 automotive benchmarking database.

Conflicts of Interest: The authors declare no conflict of interest, and the funders had no role in the design of the study; in the collection, analyses, or interpretation of data; in the writing of the manuscript; or in the decision to publish the results.

Appendix A

This appendix presents the database we used for developing our parametric models. Tables A1–A3 give an overview of the database. For each vehicle model, the brand, the ADAC model series, the production year, and the drivetrain type are listed. The ADAC Model Series column is empty for the vehicles not sold in Germany. The “Wheel model” column specifies the parametric model for which each vehicle was used.

For simplicity’s sake, we use the following abbreviations to identify the parametric models:

- All: the vehicle is used for all models;
- BV: brake volume (Section 2.2.1);
- BW: brake weight (Section 2.2.2);
- RD: minimum rim diameter (Section 2.3.1);
- RW: rim weight (Section 2.3.2);
- TW: tire weight (Section 2.4.2).

Table A1. Database overview, part 1.

Brand	Vehicle Model	ADAC Model Series	Production Year	Wheel Model
Audi	e-tron 55 quattro	e-tron (GE) (from 03/19)	2019	All
Audi	A3 Sportback e-tron	A3 (8V) Sportback e-tron (01/15–05/16)	2015	BV, RD
BAIC	EX360 Fashion	-	2018	BW, TW, RW
BMW	2 Series Active Tourer 225 xe Luxury	2-er Reihe(F45) Active Tourer (09/14-02/18)	2016	All
BMW	5 Series 530e iPerformance	5-er Reihe (G30) Limousine (from 02/17)	2018	All
BMW	i3 Range Extender Urban Life	i3 (11/13–08/17)	2014	All
BMW	i3 Range Extender	i3 (from 11/17)	2018	BV, RD
BMW	X1 xDrive 25Le	-	2018	BW, TW, RW
BMW	X5 2.0 xDrive40e	X5 (F15) (11/13–07/18)	2016	BV, RD
BYD	E6 Jingying Ban	-	2015	BW, TW, RW
BYD	Song DM 1.5 comfort	-	2017	BW, TW, RW
BYD	Tang 2.0 Ultimate	-	2015	BW, TW, RW
BYD	Tang EV 600D ChuangLing	-	2019	BW
BYD	Yuan EV 360 Cool	-	2017	BW, TW, RW
Chevrolet	Malibu Eco 2.4	-	2011	BV
Chevrolet	Volt 1.4 Voltec	Volt (11/11–08/14)	2011	All
Chevrolet	Volt 1.5 Premier	-	2015	BV
Citroen	DS5 Hybrid4 So Chic	DS 5 (03/12–05/15)	2012	All
Ford	C-Max Energi SEL 2.0	C-MAX (II) (11/10–05/15)	2013	BV
Denza	EV Executive	-	2014	BW, TW, RW
Gac Ne	Aion S Max 630	-	2019	BW
Geely	Emgrand EV300 elite	-	2015	BW, TW, RW

Table A1. Cont.

Brand	Vehicle Model	ADAC Model Series	Production Year	Wheel Model
Geometry	A Standard range power edition	-	2019	BW
Honda	CR-V 2.0 Hybrid Comfort	CR-V (V) (from 10/18)	2019	All
Hyundai	Ioniq 1.6 Plug-in	IONIQ (AE) Hybrid (10/16–07/19)	2017	All
Hyundai	Kona electric Executive 64 kWh	Kona (OS) Elektro (from 08/18)	2018	All
Jaguar	I-Pace EV 400	I-Pace (X590) (from 10/18)	2018	All

All = the vehicle is used for all models; BV = brake volume; BW = brake weight; RD = minimum rim diameter; RW = rim weight; TW = tire weight.

Table A2. Database overview, part 2.

Brand	Vehicle Model	ADAC Model Series	Production Year	Wheel Model
Kia	Niro 1.6 GDi HEV Active	Niro (DE) (09/16–05/19)	2016	All
Lexus	GS 450h F-Sport	GS (L10) (06/12–08/15)	2012	All
Maxus	EG10 Luxury		2017	BW, TW, RW
Mercedes	EQC 400 4MATIC 1886 Edition	EQC (293) (from 06/19)	2019	All
Mercedes	GLE 550e 3.0 4Matic	GLE (166) (08/15–10/18)	2016	BV, RD
Mitsubishi	I-Miev	i-MiEV (12/10–04/14)	2011	RD
Mitsubishi	Outlander PHEV Business Nav Safety	Outlander (III) Plug-In Hybrid (05/14–10/15)	2014	All
Mitsubishi	Outlander PHEV GT S-AWC	Outlander (III) Plug-In Hybrid (10/15–08/18)	2017	BV, RD
Nio	ES8 Base	-	2019	BW, TW, RW
Nio	ES8 founding	-	2019	TW, RW
Nissan	Leaf 24	Leaf (ZE0) (04/12–06/13)	2011	All
Nissan	Leaf 30	Leaf (ZE0) (06/13–11/17)	2016	BV, RD
Nissan	Leaf Tekna 40	Leaf (ZE1) (from 01/18)	2018	All
Opel	Ampera-e	Ampera-E (07/17–06/19)	2017	All
Porsche	Cayenne e-Hybrid	Cayenne (9YA) (from 11/17)	2018	All
Porsche	Cayenne S-Hybrid	Cayenne (958) (10/14–12/17)	2014	BV, RD

Table A2. Cont.

Brand	Vehicle Model	ADAC Model Series	Production Year	Wheel Model
Renault	Kangoo Maxi Z.E. 33	Kangoo (II) Z.E. Rapid (from 05/13)	2017	BW
Renault	Zoe R135 Edition One	Zoe (from 10/19)	2019	BW
Renault	Zoe ZE Intens	Zoe (06/13–09/19)	2013	All
Roewe	550 1.5 Plug-in hybrid	-	2016	BW, TW, RW
Roewe	ei5 Topline	-	2018	BW, TW, RW
Roewe	Marvel X AWD	-	2018	BW, TW, RW
Roewe	RX5 1.5 plug-in Hybrid	-	2017	BW, TW, RW
Roewe	RX5 EV400	-	2017	BW, TW, RW
Tesla	Model-S 60 kWh	Model S (08/13–04/16)	2013	BV, RD
Tesla	Model-X P90D	Model X (from 06/16)	2016	BV, RD
Toyota	Auris 1.8 HSD Dynamic nav. comfort	Auris (E18) (01/13–08/15)	2013	All
Toyota	Camry Hybrid	No match found in ADAC	2018	BV
Toyota	C-HR 1.8 Hybrid	C-HR (X10) (10/16–11/19)	2018	All
Toyota	Corolla 1.8 Hybrid elite	Corolla (E17) (12/16–12/18)	2017	All

Table A3. Database overview, part 3.

Brand	Vehicle Model	ADAC Model Series	Production Year	Wheel Model
Toyota	Corolla 2.0 Hybrid Collection	Corolla (E21) (from 04/19)	2019	All
Toyota	Levin 1.8 Hybrid CVT Zunxiang	No match found in ADAC	2018	BW, RW
Toyota	Prius 1.8 Hybrid Four Touring	Prius (XW3) (04/12–02/16)	2015	BV
Toyota	Prius 1.8 PHV	Prius (XW5) Plug-In (from 03/17)	2017	All
Toyota	Prius 1.8 Plug-in Hybrid	Prius (XW3) Plug-In (10/12–12/16)	2012	BV, RD
Toyota	Prius 1.8 VVT-i Hybrid Lounge	Prius (XW5) (from 03/16)	2016	All
Toyota	RAV4 2.5 Hybrid Lounge	RAV4 (XA5) (from 01/19)	2019	All
Volkswagen	Golf VII e-Golf 85 kW	Golf (VII) e-Golf (03/14–10/16)	2014	All
Volkswagen	Golf VII e-Golf 100 kW	Golf (VII) e-Golf (04/17–05/20)	2018	BV
Volkswagen	Golf VII GTE	Golf (VII) GTE (12/14–10/16)	2015	All
Volkswagen	Jetta Hybrid 1.4	Jetta IV (01/11–08/14)	2013	BV, RD

Table A3. Cont.

Brand	Vehicle Model	ADAC Model Series	Production Year	Wheel Model
Volkswagen	Up! e-Up!	up! e-up! (04/13–06/16)	2013	All
Volvo	XC60 2.0 T8 Twin Engine AWD R-Design	XC60 (U) (from 07/17)	2018	All
Volvo	XC90 T8 Inscription	XC90 (L) (from 01/15)	2015	BV, RD
Weltmeister	EX5 500 Extra	No match found in ADAC	2019	BW, TW, RW
Zotye	E200	No match found in ADAC	2016	BW, TW, RW

Table A4. List of employed symbols.

Symbol	Description	Unit
$m_{veh\ max}$	Vehicle gross weight	kg
$v_{veh\ max}$	Maximum vehicle speed	km/h
$t_{veh\ 0-100}$	Acceleration time from 0 to 100 km/h	s
D_{brake}	Brake disc diameter	mm
m_{brake}	Brake disc weight	kg
$D_{rim\ min\ ADAC}$	Smallest rim diameter in a model series	mm
$D_{rim\ clearance}$	Rim radial clearance	mm
m_{rim}	Rim weight	kg
D_{rim}	Rim diameter	mm or inches
D_{tire}	Tire diameter	mm
$h_{\%}$	Nominal aspect ratio	/
w_{tire}	Tire section width	mm
V_{tire}	Tire volume	mm ³
$m_{88\%}$	Loaded vehicle weight according to the 88% rule	kg
$m_{100\%}$	Loaded vehicle weight according to the 100% rule	kg
$l_{F, 88\%}$	Distance between the center of mass and the front axle for the 88% rule	mm
$l_{F, 100\%}$	Distance between the center of mass and the front axle for the 100% rule	mm
$L_{tire88\%}$	Tire load according to the 88% rule	kg
$L_{tire100\%}$	Tire load according to the 100% rule	kg
L_{tire}	Tire load	kg
V_{tireSL}	Tire volume allowing a standard-load tire to carry a given load	mm ³
V_{tireEL}	Tire volume allowing an extra-load tire to carry a given load	mm ³
m_{tire}	Tire weight	kg
$w_{wheelhouse}$	Wheelhouse width	mm
$W106$	Vehicle width at the front axle	mm
w_{srr}	Width of the side roll rail	mm
$w_{available}$	Available space at the front axle	mm
$w_{required}$	Space required by the powertrain components	mm
δ_{max}	Maximum wheel steering angle	deg
$R_{turning}$	Vehicle turning radius	mm
$L101$	Vehicle wheelbase	mm
$L104$	Vehicle front overhang	mm
$W103$	Vehicle maximum width (without side mirrors)	mm
$W101$	Vehicle front track width	mm
m_{BIW}	BIW weight	kg
V_{veh}	Vehicle volume	m ³
$L105$	Vehicle rear overhang	mm
$H100$	Vehicle height	mm

BIW = body in white.

Table A5. Database for the evaluation of the wheel model.

Brand	ADAC Model Series	VCW in kg	VGW in kg
Audi	e-tron (GE) (from 03/2019)	2565	3130
BMW	2er-Reihe (F45) Active Tourer (09/14–02/18)	1735	2180
BMW	5er-Reihe (G30) Limousine (from 02/17)	1845	2440
BMW	i3 (11/13–08/17)	1415	1755
BMW	X5 (F15) (11/13–07/18)	2305	2980
Hyundai	IONIQ (AE) Hybrid (10/16–07/19)	1580	1970
Hyundai	Kona (OS) Elektro (from 08/18)	1760	2170
Jaguar	I-Pace (X590) (from 10/18)	2208	2670
Kia	Niro (DE) (09/16–05/19)	1594	2000
Mitsubishi	Outlander (III) Plug-In Hybrid (05/14–10/15)	1945	2310
Nissan	Leaf (ZE1) (from 01/18)	1707	2140
Opel	Ampera-E (07/17–06/19)	1691	2056
Porsche	Cayenne (9YA) (from 11/17)	2370	3030
Renault	Zoe (06/13–09/19)	1575	1954
Toyota	Auris (E18) (01/13–08/15)	1420	1915
Toyota	C-HR (X10) (10/16–11/19)	1460	1930
Toyota	Prius (XW5) Plug-In (from 03/17)	1605	1855
Toyota	Prius (XW3) Plug-In (10/12–12/16)	1500	1840
Toyota	RAV4 (XA5) (from 01/19)	1795	2185
VW	Golf VII e-Golf (03/14–10/16)	1585	1980
VW	up! e-up! (04/13–06/16)	1215	1500
Volvo	XC60 (U) (from 07/17)	2223	2660
Volvo	XC90 (L) (from 01/15)	2384	3010

References

1. The European Parliament and the Council of the European Union. Regulation (EU) 2019/631 of the European Parliament and of the Council of 17 April 2019 setting CO₂ emission performance standards for new passenger cars and for new light commercial vehicles, and repealing Regulations (EC) No 443/2009 and (EU) No 510/2011. *Off. J. Eur. Union* **2019**, *111*, 13–53. Available online: <https://eur-lex.europa.eu/legal-content/EN/TXT/?uri=CELEX%3A32019R0631> (accessed on 13 June 2020).
2. The International Council on Clean Transportation. *CO₂ Emission Standards for Passenger Cars and Light-Commercial Vehicles in the European Union*; ICCT: Washington, DC, USA, 2019; Available online: https://theicct.org/sites/default/files/publications/EU-LCV-CO2-2030_ICCTupdate_201901.pdf (accessed on 21 June 2020).
3. Nicoletti, L.; Mayer, S.; Brönnner, M.; Schockenhoff, F.; Markus, L. Design Parameters for the Early Development Phase of Battery Electric Vehicles. *WEVJ* **2020**, *11*, 47. [CrossRef]
4. ADAC. VW e-Golf (04/17–05/20): Technische Daten, Preise. Available online: <https://www.adac.de/rund-ums-fahrzeug/autokatalog/marken-modelle/vw/golf/vii-facelift/266575/#> (accessed on 7 June 2020).
5. ADAC. VW Golf 1.0 TSI BMT Trendline (03/17–08/18). Available online: <https://www.adac.de/rund-ums-fahrzeug/autokatalog/marken-modelle/vw/golf/vii-facelift/266199/#> (accessed on 7 June 2020).
6. Fuchs, S. Verfahren zur parameterbasierten Gewichtsabschätzung neuer Fahrzeugkonzepte: Ein Werkzeug zur Spezifikation von effizienten Antriebstopologien für Elektrofahrzeuge. Ph.D. Thesis, Technical University of Munich, Munich, Germany, 2014. Available online: <https://mediatum.ub.tum.de/1207264> (accessed on 4 June 2020).
7. Yanni, T.; Venhovens, P.J.T. Impact and Sensitivity of Vehicle Design Parameters on Fuel Economy Estimates. In Proceedings of the SAE 2010 World Congress & Exhibition, Detroit, MI, USA, 13–15 April 2010. [CrossRef]
8. Mau, R.J.; Venhovens, P.J. Parametric vehicle mass estimation for optimization. *Int. J. Veh. Des.* **2016**, *72*, 1–16. [CrossRef]
9. Felgenhauer, M.; Nicoletti, L.; Schockenhoff, F.; Angerer, C.; Lienkamp, M. Empiric Weight Model for the Early Phase of Vehicle Architecture Design. In Proceedings of the 2019 Fourteenth International Conference on Ecological Vehicles and Renewable Energies (EVER), Monte-Carlo, Monaco, 8–10 May 2019. [CrossRef]

10. Alonso, E.; Lee, T.M.; Bjelkengren, C.; Roth, R.; Kirchain, R.E. Evaluating the potential for secondary mass savings in vehicle lightweighting. *Environ. Sci. Technol.* **2012**, *46*, 2893–2901. [[CrossRef](#)] [[PubMed](#)]
11. Wiedemann, E.; Meurle, J.; Lienkamp, M. Optimization of Electric Vehicle Concepts Based on Customer-Relevant Characteristics. *SAE Tech. Pap. Ser.* **2012**. [[CrossRef](#)]
12. Wiedemann, E. Ableitung von Elektrofahrzeugkonzepten aus Eigenschaftszielen. Ph.D. Thesis, Technical University of Munich, Munich, Germany, 2014.
13. Fuchs, S.; Lienkamp, M. Parametric Modelling of Mass and Efficiency of New Vehicle Concepts. *ATZ Worldw.* **2013**, *115*, 60–66. [[CrossRef](#)]
14. Angerer, C.R. Antriebskonzept-Optimierung für Batterieelektrische Allradfahrzeuge. Ph.D. Thesis, Technical University of Munich, Munich, Germany, 2020.
15. Angerer, C.; Krapf, S.; Buß, A.; Lienkamp, M. Holistic Modeling and Optimization of Electric Vehicle Powertrains Considering Longitudinal Performance, Vehicle Dynamics, Costs and Energy Consumption. In Proceedings of the ASME International Design Engineering Technical Conferences and Computers and Information in Engineering Conference, Quebec City, QC, Canada, 26–29 August 2018. [[CrossRef](#)]
16. Del Pero, F.; Berzi, L.; Antonacci, A.; Delogu, M. Automotive Lightweight Design: Simulation Modeling of Mass-Related Consumption for Electric Vehicles. *Machines* **2020**, *8*, 51. [[CrossRef](#)]
17. Leebmann24.de. BMW Online Shop. Originalprodukte Online Kaufen—Leebmann24.de. Available online: <https://www.leebmann24.de/#> (accessed on 15 May 2020).
18. Continental AG. Reifen von Continental. Available online: <https://www.continental-reifen.de/autoreifen/reifen?cartype=car&season=summer#> (accessed on 20 April 2020).
19. A2mac1. a2mac1 Automotive Benchmarking. Available online: <https://portal.a2mac1.com/de/home-2/#> (accessed on 1 February 2020).
20. ADAC. Allgemeine Deutsche Automobilclub. Available online: <https://www.adac.de/#> (accessed on 14 March 2020).
21. ADAC. Audi e-tron 1.Generation: Technische Daten, Preise. Available online: <https://www.adac.de/rundums-fahrzeug/autokatalog/marken-modelle/audi/e-tron/1generation/#> (accessed on 27 May 2020).
22. German Institute for Standardization. *DIN 70020-3:2008-03. Road Vehicles—Automotive Engineering—Part 3: Testing Conditions, Maximum Speed, Acceleration and Elasticity, Mass, Terms, Miscellaneous*; German Institute for Standardization: Berlin, Germany, 2008.
23. Bundesministerium der Justiz und für Verbraucherschutz. Straßenverkehrs-Zulassungs-Ordnung (StVZO): §34 Achslast und Gesamtgewicht. Available online: https://www.gesetze-im-internet.de/stvzo_2012/_34.html# (accessed on 20 April 2020).
24. Reif, K. *Bremsen und Bremsregelsysteme*; Vieweg+Teubner Verlag: Wiesbaden, Germany; GWV Fachverlage GmbH: Wiesbaden, Germany, 2010; ISBN 978-3-834-81311-4.
25. Duval-Destin, M.; Kropf, T.; Abadie, V.; Fausten, M. Auswirkungen eines Elektroantriebs auf das Bremssystem. *ATZ Automob. Z* **2011**, *113*, 638–643. [[CrossRef](#)]
26. Wagner, D.; Hoffmann, J.; Lienkamp, M. Downsizing potential of wheel brakes in electric vehicles. In Proceedings of the 8th International Munich Chassis Symposium, Munich, Germany, 20–21 June 2017; pp. 661–691. [[CrossRef](#)]
27. UN/ECE. Regulation No 13-H of the Economic Commission for Europe of the United Nations (UN/ECE)—Uniform provisions concerning the approval of passenger cars with regard to braking. *Off. J. Eur. Union* **2015**, *335*, 1–84. Available online: <https://eur-lex.europa.eu/legal-content/EN/TXT/?uri=CELEX%3A42015X1222%2801%29> (accessed on 30 May 2020).
28. Doerr, J.; Ardey, N.; Mendl, G.; Fröhlich, G.; Straßer, R.; Laudenbach, T. The new full electric drivetrain of the Audi e-tron. In *Der Antrieb von Morgen 2019*; Springer Vieweg: Wiesbaden, Germany, 2019; pp. 13–37. [[CrossRef](#)]
29. Dietz, J.; Helmers, E.; Türk, O.; Beringer, F.; Brand, U.; Walter, J. Ökobilanzierung von Elektrofahrzeugen. Available online: https://www.stoffstrom.org/fileadmin/userdaten/dokumente/Netzwerk_Elektromobilitaet/8a_Oekobilanzierung_von_Elektrofahrzeugen_Netzwerk_E-Mobilitaet_RLP.pdf# (accessed on 1 June 2020).
30. Breuer, B. *Bremsenhandbuch: Grundlagen, Komponenten, Systeme, Fahrdynamik*; Vieweg Verlag: Wiesbaden, Germany, 2004; ISBN 978-3-322-99536-0.
31. Textar Brake Technology. Benchmark Testing: Ams-Test: The Test: Do the Pads Perform When Hot and Cold? Available online: <https://textar.com/en/ams-test/#> (accessed on 15 July 2020).

32. European Tyre and Rim Technical Organisation (ETRTO). Standards Manual: ETRTO—The European Tyre and Rim Technical Organisation. 2014. Available online: <https://www.etrto.org/Publications/Available/Standards-Manual> (accessed on 22 May 2020).
33. Luccarelli, M.; Lienkamp, M.; Matt, D.; Spena, P.R. Automotive Design Quantification: Parameters Defining Exterior Proportions According to Car Segment. *SAE Tech. Pap. Ser.* **2014**. [CrossRef]
34. Leister, G. *Passenger Car Tires and Wheels: Development—Manufacturing—Application*; Springer International Publishing: Cham, Switzerland, 2018; ISBN 978-3-319-50117-8.
35. Jazar, R.N. *Vehicle Dynamics: Theory and Application*; Springer International Publishing: Cham, Switzerland, 2017; ISBN 978-3-319-53440-4.



© 2020 by the authors. Licensee MDPI, Basel, Switzerland. This article is an open access article distributed under the terms and conditions of the Creative Commons Attribution (CC BY) license (<http://creativecommons.org/licenses/by/4.0/>).